

## Article

# Paper-Based Electrodes Conjugated with Tungsten Disulfide Nanostructure and Aptamer for Impedimetric Detection of *Listeria monocytogenes*

Annu Mishra <sup>1</sup>, Roberto Pilloton <sup>2,\*</sup>, Swati Jain <sup>1</sup>, Souradeep Roy <sup>3</sup>, Manika Khanuja <sup>4</sup>, Ashish Mathur <sup>3</sup> and Jagriti Narang <sup>5</sup>

- <sup>1</sup> Amity Institute of Nanotechnology, Amity University, Noida 201313, India; annum407@gmail.com (A.M.); swatijain.iitd@gmail.com (S.J.)
- <sup>2</sup> CNR-IC, Area della Ricerca di RM1, Via Salaria km 29.3, Monterotondo, I-00015 Rome, Italy
- <sup>3</sup> Centre for Interdisciplinary Research and Innovation (CIDRI), University of Petroleum and Energy Studies, Dehradun 248007, India; roysouradeep04@gmail.com (S.R.); nanoashish@gmail.com (A.M.)
- <sup>4</sup> Centre for Nanoscience and Nanotechnology, Jamia Millia Islamia, New Delhi 110025, India; manikakhanuja@gmail.com
- <sup>5</sup> Department of Biotechnology, Jamia Hamdard, New Delhi 110062, India; jags\_biotech@yahoo.co.in
- \* Correspondence: roberto.pilloton@cnr.it

**Abstract:** In this study, we report on a novel aptasensor based on an electrochemical paper-based analytical device (ePAD) that employs a tungsten disulfide (WS<sub>2</sub>)/aptamer hybrid for the detection of *Listeria monocytogenes*. *Listeria* is a well-known causative pathogen for foodborne diseases. The proposed aptasensor signifies many lucrative features which include simple, cost-effective, reliable, and disposable. Furthermore, the use of an aptamer added more advantageous features in the biosensor. The morphological, optical, elemental composition, and phase properties of the synthesized tungsten disulfide (WS<sub>2</sub>) nanostructures were characterized by field-emission scanning electron microscopy (FESEM), RAMAN spectroscopy, photoluminescence (PL), and X-ray diffraction (XRD), while electrochemical impedance spectroscopy was performed to corroborate the immobilization of aptamer and to assess the *L. monocytogenes* sensing performance. The limit of detection (LoD) and limit of quantification (LoQ) of the aptasensor was found to be 10 and 4.5 CFU/mL, respectively, within a linear range of 10<sup>1</sup>–10<sup>8</sup> CFU/mL. The proposed sensor was found to be selective solely towards *Listeria monocytogenes* in the presence of various bacterial species such as *Escherichia coli* and *Bacillus subtilis*. Validation of the aptasensor operation was also evaluated in real samples by spiking them with fixed concentrations (10<sup>1</sup>, 10<sup>3</sup>, and 10<sup>5</sup>) of *Listeria monocytogenes*, thereby, paving the way for its potential in a point-of-care scenario.



**Citation:** Mishra, A.; Pilloton, R.; Jain, S.; Roy, S.; Khanuja, M.; Mathur, A.; Narang, J. Paper-Based Electrodes Conjugated with Tungsten Disulfide Nanostructure and Aptamer for Impedimetric Detection of *Listeria monocytogenes*. *Biosensors* **2022**, *12*, 88. <https://doi.org/10.3390/bios12020088>

Received: 30 December 2021

Accepted: 21 January 2022

Published: 31 January 2022

**Publisher's Note:** MDPI stays neutral with regard to jurisdictional claims in published maps and institutional affiliations.



**Copyright:** © 2022 by the authors. Licensee MDPI, Basel, Switzerland. This article is an open access article distributed under the terms and conditions of the Creative Commons Attribution (CC BY) license (<https://creativecommons.org/licenses/by/4.0/>).

**Keywords:** ePAD; *Listeria monocytogenes*; WS<sub>2</sub> nanoparticles; paper-based electrode; electrochemical aptasensor; point-of-care

## 1. Introduction

Foodborne pathogens have proven to be a severe threat to the food industries that deal with important public health crises across the world [1]. According to the World Health Organization (WHO), foodborne diseases affect approximately one-third of the population in developed countries annually, while this ratio is even higher in developing nations [2]. Bacteria such as *Listeria monocytogenes*, a harmful organism (e.g., human listeriosis), is a considerable concern for pregnant women, infants, and adults who are suffering from a weak immune system [3]. *L. monocytogenes* is associated with the consumption of raw and undercooked meat, poultry food, unpasteurized milk, cheese, and other dairy products. Furthermore, reports have suggested that death rates due to *L. monocytogenes* surged between 2001 and 2009 [4,5]. Therefore, the consequences associated with this bacterium are the foremost concern in food industry treatments.

Detection of pathogenic bacteria can be done through conventional techniques that involve a culture-based approach or a combination of a culture-based approach with numerous biochemical assays [6]. In spite of being highly precise and possessing the ability to distinguish between live and dead cells, such assays are bulky, non-specific, less sensitive, time-consuming, lengthy experimental procedures, lack quantitative results, and are unfeasible for point-of-care applications [7]. Due to these limitations, there is an extensive requirement to develop a suitable approach that can address the wide gaps in the existing detection methods.

Electrochemical biosensors have been incorporated as an alternative approach to overcome the drawbacks of traditional methods for foodborne pathogen monitoring, with the focus on being faster, cheaper, and real-time detection [8]. In the present era, an electrochemical biosensor matrix plays an essential role in improving a highly selective, reliable, sensitive and cost-effective analysis for clinical diagnosis [9]. Metallic nanostructures can be incorporated as electrode surface modifiers because they offer high electric conductivity due to quantum confinement effects [10]. Such a property is desirable for enhancing interfacial electron transfer kinetics.

In the present approach, we emphasize the fabrication of a label-free impedimetric aptasensor to detect *Listeria monocytogenes*. Construction of an electrochemical aptasensor involves using a paper-based device with advantageous features such as a low volume of analytes, mass-producible, lightweight, flexible, affordability, disposable, and rapidity, along with the feasibility of liquid flow without any external perturbation. The abovementioned advantages of electrochemical paper analytical devices (ePADs) make them a cheap platform for use in a resource-limited environment [11]. Specifically, the working electrode of an ePAD was modified with tungsten disulfide ( $WS_2$ ) due to its biocompatibility and higher electron transfer to enhance the electrochemical signals. Furthermore, the aptamer modified with amine groups was immobilized on the surface-modified working electrode of the ePAD and an electrochemical analysis was performed to confirm the respective hybridization. In our current study, the aptamer was selected based on the work done by Sidhu et al. [11] and was exploited to fabricate a biosensor [12].

In this research, we report on the analytical performance of a  $WS_2$ /aptamer hybrid-based aptasensor towards the selective detection of *Listeria monocytogenes* in an experimentally synthesized electrolyte as well as spiked dairy products, thereby, validating the developed sensor as a potential candidate for specific and sensitive bacterial detection.

## 2. Materials and Methods

### 2.1. Reagents

Sodium tungstate ( $Na_2WO_4$ ), thiourea ( $CH_4N_2S$ ), and methylene blue (MB) were purchased from Fisher Scientific, Pvt. Ltd., New Delhi, India. Hydroxylamine hydrochloride ( $HONH_2 \cdot HCl$ ), polyethylene glycol ( $C_{2n}H_{4n+2}O_{n+1}$ ), potassium chloride (KCl), sodium monobasic ( $NaH_2PO_4$ ), and dibasic salts ( $Na_2HPO_4$ ) were purchased from Central Drug House (CDH), Pvt. Ltd., New Delhi, India.  $NaH_2PO_4$  and  $Na_2HPO_4$  were used in the preparation of phosphate buffer saline (PBS, 0.1 M and pH 7.4). Tris HCl-EDTA (TE buffer) was used to prepare the aliquot of the oligonucleotides and, afterwards, stored at 4 °C. All the chemicals used were prepared in double distilled water (DDW).

Aliquots of bacterial strains used, in this study, were acquired from the Culture Collection (*Listeria monocytogenes* strains), Microbial Type Culture Collection, and Gene Bank CSIR-IMTECH, Chandigarh (1143-*L. monocytogenes*). *E. coli* and *B. subtilis* were cultured in sterilized conditions at the Amity University, Amity Institute of Biotechnology, Noida.

The amine-modified sequence of *L. monocytogenes* was synthesized by GCC Biotech (Pvt. Ltd., Delhi, India). The 47-mer aptamer sequence of *Listeria* was obtained from Sidhu, R. et al. [11], i.e., -5'-NH<sub>2</sub>-ATC CAT GGG GCG GAGATG AGG GGG AGG AGG GCG GGT ACC CGG TTGAT-3'.

## 2.2. Apparatus

Electrochemical impedance spectroscopy was performed using a Wayne Kerr 6500-B Precision Impedance Analyzer for sensing of *L. monocytogenes* on WS<sub>2</sub>/aptamer modified electrodes. The ePAD involved a two-electrode system that was fabricated by screen printing conductive carbon ink on 210 GSM sheets. The working region of the ePAD was incorporated with WS<sub>2</sub> nanostructures (WS<sub>2</sub>NS) as a biocompatible and enhanced electron conductivity matrix to detect *L. monocytogenes*.

The morphology of the synthesized WS<sub>2</sub> nanostructure was characterized by FE-SEM (Zeiss 18448), while the molecular fingerprints of the WS<sub>2</sub> nanostructures were analyzed by RAMAN spectroscopy (Shimadzu 8700), in the region of 500–4500 cm<sup>-1</sup>. The X-ray diffraction patterns (RigakuXRD, Smart Lab) were recorded in the range of 10° to 80° using CuK $\alpha$  radiation (40 kV, 30 mA) to investigate the crystal structure of WS<sub>2</sub>. The photoluminescence (PL) spectroscopy was performed using a RF5301-PC SHIMAZZU spectrofluorometer to analyze the defect structure of the synthesized nanomaterial. The PL spectra were recorded at the excitation wavelength of 650 nm with 300 to 800 nm of scanning through a 1.0 nm step length.

## 2.3. Bacteria Culture

The cultivation of pathogenic strains was performed in Luria broth (LB) medium at 37 °C by stirring for 16 h at 170 rpm. Bacterial cultures were centrifuged at 5800 r/min for 10 min (25 °C) and washed thrice by PBS (0.1 M, pH 7.4). The resulting precipitate was mixed in 15 mL of PBS as the initial stock solution of *L. monocytogenes*. The bacteria concentrations were prepared by serial dilution in PBS, while the corresponding absorbance was measured at 600 nm. Then, the original bacterial aliquot was further diluted to prepare concentrations from 10<sup>1</sup> to 10<sup>8</sup> CFU/mL

## 2.4. Synthesis of Tungsten Disulfide (WS<sub>2</sub>) Nanoflakes

Sodium tungstate (4.74 g), thiourea (4.5 g), hydroxylamine hydrochloride (2.06 g), and PEG (0.54 g) were added to 90 mL of deionized (DI) water under constant stirring in a beaker for 1h. The prepared solutions were transferred to a 150 mL Teflon-lined autoclave and kept at 180 °C for 24 h. After 24 h, the autoclave was allowed to cool down at room temperature. The obtained sample was subjected to vacuum filtration using Whatman filter paper. The filtrate was washed several times with ethanol and DI water, followed by drying at 40 °C for 4h. The obtained sample was ground to form a fine powder.

## 2.5. Development of Paper-Based Sensor Drop Cast with Tungsten Disulfide Nanoflakes (WS<sub>2</sub>NFs)

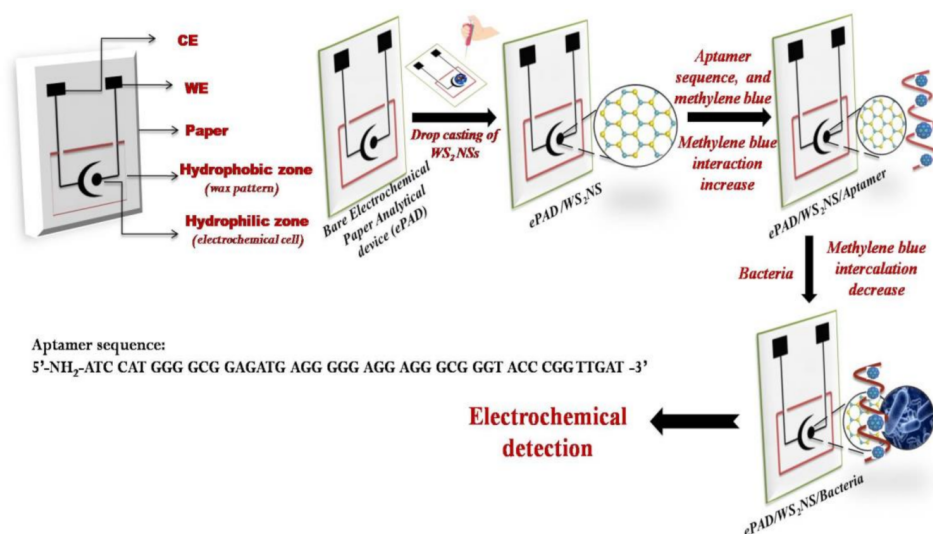
The electrochemical paper-based micro-analytical device (ePAD) was fabricated via screen printing technology using carbon conductive ink, as reported in the literature [13,14]. After drying the ink for 20 min, a wax coating was applied around the electrodes to create a hydrophobic barrier and to define the working area over the ePAD. Further, the working electrodes were modified with WS<sub>2</sub> nanostructure (10  $\mu$ L) drop cast on the ePAD and were dried at 25 °C, followed by immobilization of 5  $\mu$ L aptamer (20  $\mu$ M), and allowed to stabilize for overnight at 4 °C.

## 2.6. Fabrication of *Listeria* Aptamer ssDNA/WS<sub>2</sub>NF/ePAD

In order to fabricate the *Listeria* aptamer single-stranded DNA/WS<sub>2</sub>NF/ePAD modified electrode, various concentrations (20, 40, 60, 80, and 100  $\mu$ M) of specific aptamer sequences of *L. monocytogenes* were optimized. The dilution made different concentrations of the initial 100  $\mu$ M ssDNA solution with Tris-EDTA (TE) buffer.

The ssDNA aptamer (5'-NH<sub>2</sub>-ATC CAT GGG GCG GAGATG AGG GGG AGG AGG GCG GGT ACC CGG TTGAT-3') of *L. monocytogenes* (5  $\mu$ L) was immobilized on the WS<sub>2</sub>NF-coated ePAD, at 4 °C for 1 h. The electrochemical impedance spectroscopy studies were recorded using 0.1 M KCl electrolyte with 0.1 mM MB. The performance of the aptasensor

was analyzed by exposing it to solutions consisting of various concentrations of the bacteria. The overall process is summarized in Scheme 1.



**Scheme 1.** Schematic representation of the fabrication of the screen-printed paper-based aptasensor for the detection of *Listeria monocytogenes*.

### 2.7. Bacteria Detection

First, the sensor was incubated using *Listeria* concentration ( $10^8$  CFU/mL) at  $37^\circ\text{C}$  until the bacteria bound completely (30 min) with corresponding aminated aptamer. Then, the EIS analysis was performed in 0.1 M KCl containing 0.1 mM MB.

Control bacteria such as *E. coli* and *B. subtilis* were employed for the specificity and standard experiments. The fabrication was the same for *L. monocytogenes* (target) detection as procedure followed in aptamer fabrication. Then, each bacterium, apart from *Listeria* to detect specificity and along with bacteria to detect selectivity, was used for the electrochemical detection at the same concentration ( $10^8$  CFU/mL).

### 2.8. Repeatability and Storage Stability

The repeatability of the aptasensor was checked three times on the same day (intra-day) and duplicate measurements were performed under the same conditions after three days (inter-day) and employed for the detection of the same target bacteria concentration. The fabricated ePAD incorporated with nanomaterial was checked for 20 days at regular intervals of five days, after storage at  $4^\circ\text{C}$  for the analysis of long-term stability.

### 2.9. Application of ssDNA/WS<sub>2</sub>NS/ePAD in Food Samples

The developed aptasensor was also exposed to food sources of *L. monocytogenes*, such as unpasteurized milk and soft cheese made from unpasteurized milk. In the current process, dilutions of dairy products were done with 5 mL PBS (pH 7.4). The prepared samples were further centrifuged for 10 min at 10,000 rpm. Bacteria were spiked in dairy samples to assess the performance of the aptasensor. Afterward, the EIS study was performed to detect *L. monocytogenes* in the presence of *E. coli* and *B. subtilis* in the respective dairy sample on the aptamer-modified ePAD electrode surface.

## 3. Results and Discussion

### 3.1. Surface Characterization of WS<sub>2</sub> Nanostructures

The morphological and structural properties of synthesized WS<sub>2</sub> were performed by FESEM, XRD, RAMAN, and PL. The SEM micrograph shown in Figure 1a indicates the randomly distributed, densely packed flaky morphology of WS<sub>2</sub> nanostructures. The length and width of the flakes were measured to be  $\sim 400$  and  $200$  nm, respectively. Figure 1b shows the Raman spectrum of as-synthesized WS<sub>2</sub> nanostructures. The Raman spectrum

depicted  $E_{2g}^1$  and  $A_{1g}$  which are two active modes. The  $E_{2g}^1$  mode arises from in-phase vibrations of W atoms in the opposite direction with respect to S atoms, while the  $A_{1g}$  mode is assigned to the S atoms which are moving in-phase and in out-of-plane directions. We observed the  $E_{2g}^1$  mode at  $351\text{ cm}^{-1}$  and the  $A_{1g}$  mode at  $420\text{ cm}^{-1}$ ; the difference between these two modes, i.e.,  $\Delta\omega$  was  $69\text{ cm}^{-1}$ , which confirmed the formation of  $\text{WS}_2$  [13].

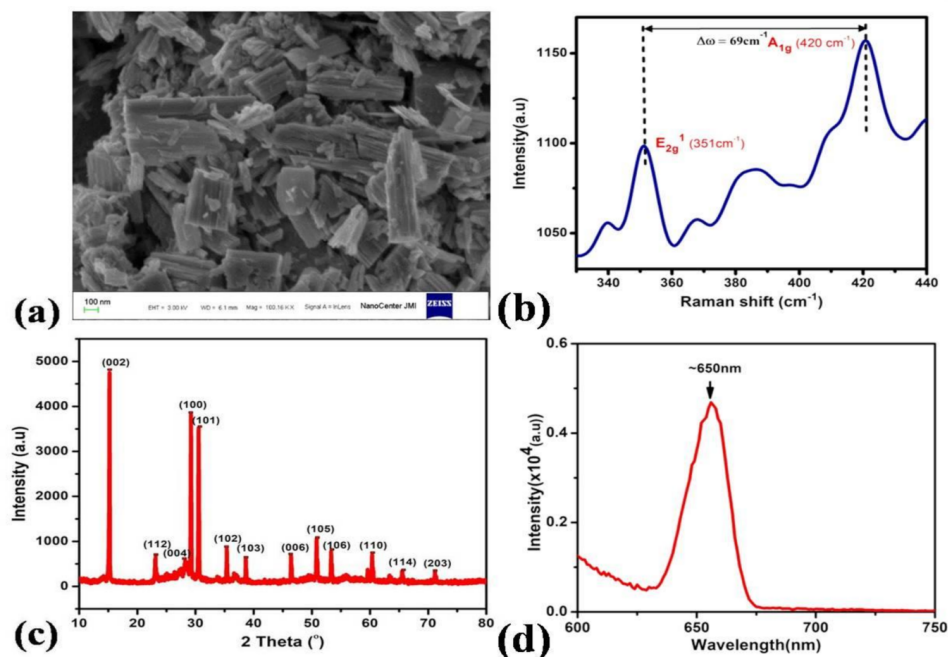


**Figure 1.** (a) SEM images; (b) Raman spectrum; (c) XRD; (d) magnified image of PL spectrum  $\text{WS}_2\text{NS}$ .

The diffraction peaks of  $\text{WS}_2$  with their respective (hkl) planes were obtained at  $15.09^\circ$  (002),  $23.4^\circ$  (112),  $28.2^\circ$  (004),  $29.2^\circ$  (100),  $30.5^\circ$  (101),  $35.3^\circ$  (102),  $38.64^\circ$  (103),  $46.4^\circ$  (006),  $50.82^\circ$  (105),  $53.22^\circ$  (106),  $59.55^\circ$  (110),  $65.51^\circ$  (114), and  $71.22^\circ$  (203), which confirmed the formation of  $\text{WS}_2$  with hexagonal structure (JCPDS No.84-1398, 08-0237) (Figure 1c). A sharp peak (002) indicated the highly crystalline nature of synthesized  $\text{WS}_2$  [13,15], while the small one at  $23.41^\circ$  was due to the organic moiety of polyethylene glycol (PEG), which was used as a surfactant.

Figure 1d shows the PL spectra of  $\text{WS}_2$  nanostructures for the evaluation of band gap and structural defects. The peak around 650 nm is attributed to the direct band-edge transition from conduction band minima to valence band maxima and the corresponding bandgap is 1.9 eV [16].

### 3.2. Electrochemical Characterization of ePADs

An EIS analysis was performed to characterize the stepwise assembly of the ePADs obtained after modification with  $\text{WS}_2\text{NS}$ , aptamer ssDNA, or bacteria in 0.1 M KCl with MB(0.1 mM). The Nyquist spectra (shown in Figure 2a–c) indicate a semicircular feature with a halfarc arising at the high-frequency region at the left side of each spectrum. The high-frequency region essentially gives the bulk electrode/electrolyte signature, in which case, the halfarc indicates a low capacitance (C), as corroborated by high-capacitive impedance  $Z''$  (since  $Z'' \propto C^{-1}$ ) [17].

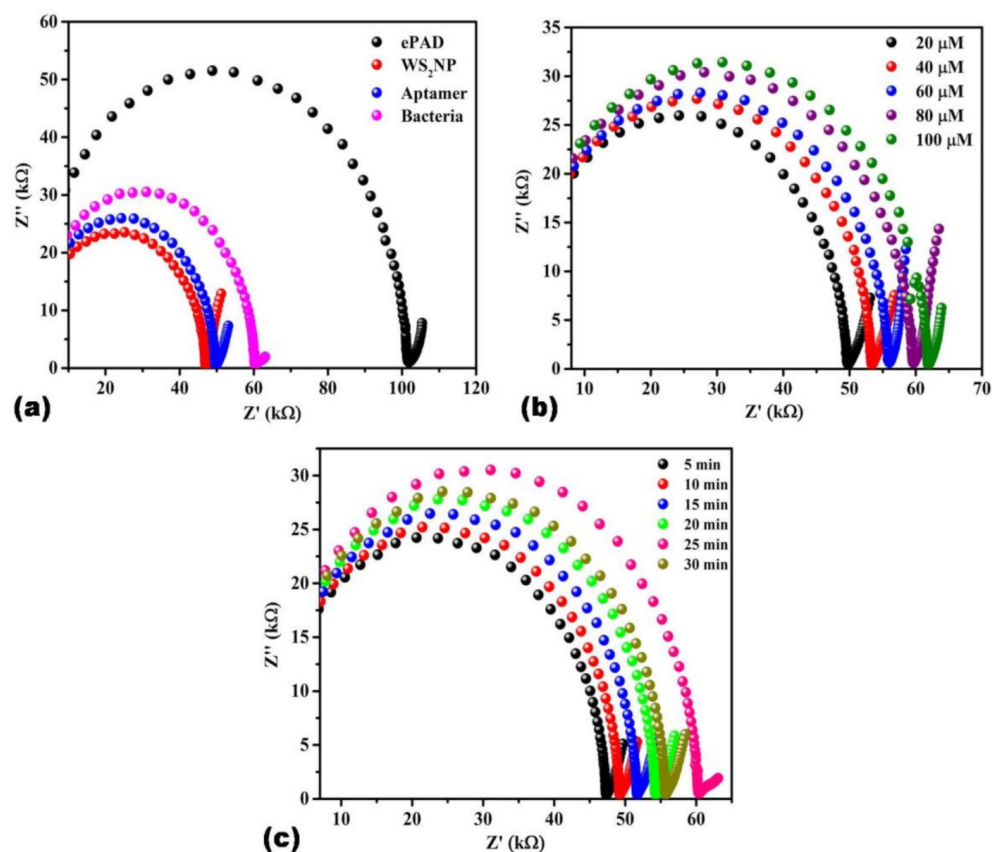


**Figure 2.** (a) Nyquist plot of a range of electrochemical paper analytical devices (ePADs) consists of ePAD,  $WS_2$ NS/ePAD, aptamer/ $WS_2$ NS/ePAD, and bacteria/aptamer/ $WS_2$ NS/ePAD; (b) Nyquist plot of aptamer/ $WS_2$ NS/ePAD at different concentrations of probe aptamer ranging from 20  $\mu M$  to 100  $\mu M$ ; (c) Nyquist plot at different incubation times in 0.1 M KCl containing 0.1 mM methylene blue (frequency range of 100 Hz–10 MHz).

It is possible to speculate that the initial low capacitance could be a signature of the screen-printed paper electrode, whereby, the poor dielectric constant ( $C \propto \epsilon$ ) of the base cellulose sheet appears to contribute towards poor charge storage ability at higher frequencies [18]. Moreover, the Nyquist spectrum seems to be shifted to the right along the  $Z'$  axis which indicates the presence of bulk resistance of base electrode and electrolyte, the latter consisting of 0.1 mM methylene blue probe in 0.1 M KCl [19]. The spectrum can be modeled by a series of resistance  $R_s$  (see Randel's circuit of Figure 3a). Furthermore, the mid-frequency region gives a measure of heterogeneous electron transfer kinetics, which is the redox process of methylene blue probe (0.1 mM in 0.1 M KCl). The electrode/electrolyte interface can be modeled using a parallel combination of resistor (indicating charge transfer resistance,  $R_{ct}$ ) and double-layer capacitance ( $C_{dl}$ ), as corroborated by the presence of a typical semicircular feature in the mid-frequency spectra. This situation denotes a turnover of electron traversal from capacitive to resistive paths since the latter is effectively dominant at low frequencies. Therefore, the parallel arrangement ensures two possible pathways for electron flow, which occur via the capacitive approach at higher frequencies ( $Z'' \propto f^{-1}$ ) and through the resistor at low frequencies [20]. Finally, the low-frequency region indicates the occurrence of diffusion-mediated transport of methylene blue probe towards the electrode surface for undergoing its signature redox process, thereby, generating electrons at the electrode/electrolyte interface.

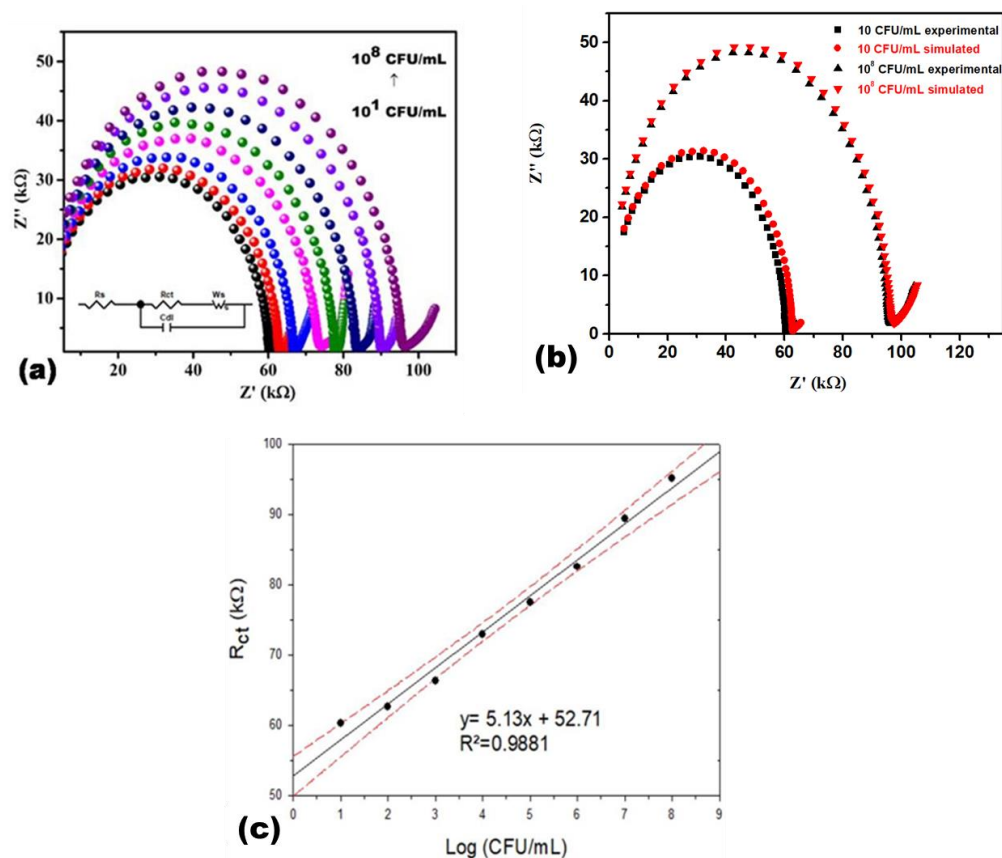


**Figure 3.** (a) Nyquist plot of bacteria/Aptamer/WS<sub>2</sub>NS/ePAD at various bacteria concentrations ( $10^1$  to  $10^8$ ). The Randel's equivalent circuit is shown in the inset; (b) curve fitting of Nyquist spectra using circuit simulation of Randel's equivalent model; (c) sensor calibration line with confidence intervals (95%) for calculation of LOD and LOQ with the graphical method by Meier and Zund, indicating direct dependence of the  $R_{ct}$  on bacteria concentrations, in 0.1 M KCl containing 0.1 mM methylene blue (frequency range of 100 Hz–10 MHz).

Now, Figure 2a depicts the Nyquist plot at different stages of electrode fabrication which shows a huge  $R_{ct}$  of  $\sim 101.91$  k $\Omega$  for the bare ePAD but a similar semi-circle with lower  $R_{ct}$  value ( $\sim 46.441$  k $\Omega$ ) for the WS<sub>2</sub>NS/ePAD. After immobilization of aptamers onto WS<sub>2</sub>NS, the  $R_{ct}$  value increased due to the non-conductive nature of aptamers, along with the repulsion between negatively charged sequence and ions present in the electrolyte. After incubation with bacteria, the resistance increased due to the non-conductive nature of bacteria bonded to the aptamer. The EIS results endorse the successful fabrication of the aptasensor.

Figure 2b shows the impedance response of modified electrodes against different aptamer concentrations. During this experiment, it was observed that the  $R_{ct}$  was the least at 20  $\mu$ M concentration and increased further with increasing concentration of aptamer. The intensification in  $R_{ct}$  value with increasing aptamer concentration ascribed to the deposition of a more insulating layer of DNA aptamer onto the working surface of ePAD. Therefore, further studies were performed at a lower aptamer concentration (20  $\mu$ M).

A time-dependent study for the sensor fabrication of ePAD was also performed. The effects are shown in Figure 2c at different immobilization times (5, 10, 15, 20, 25, and 30 min) by incubating the bacteria/aptamer/WS<sub>2</sub>NS/ePAD. The impedimetric response obtained after incubating for 25 and 30 min differed insignificantly due to the enhanced binding between the aptamer and bacteria. Therefore, the optimum time was chosen to be 25 min, as sufficient interaction of bacteria with the aptamer.

### 3.3. Electrochemical Impedance Spectroscopic Analysis of *Listeria monocytogenes*

Different concentrations ( $10^1$ ,  $10^2$ ,  $10^3$ ,  $10^4$ ,  $10^5$ ,  $10^6$ ,  $10^7$ , and  $10^8$  CFU/mL) of bacteria were incubated on the modified ePAD and the results are shown in Figure 3a. It is interesting to note that the Nyquist profile at various *L. monocytogenes* target concentrations retain the features shown in Figure 2a–c. Specifically, the low capacitance due to the poor dielectric constant of paper substrate and bulk electrode/electrolyte resistance at high frequencies, the mid-frequency interface kinetics, and low frequency methylene blue diffusion appear to be preserved in the concentration scan, which essentially indicates the stability of the fabricated aptamer/WS<sub>2</sub> bio-nano hybrid-coated ePAD.

During the apta-recognition process, as the bacterial concentration is increased, more of the bacteria becomes bonded to the probe-aptamer sites and passivates the electrode surface due to the insulating nature of bacteria [21], and the interfacial charge transfer is drastically reduced. This is indicated in Figure 3a by an increase in  $R_{ct}$  from ~58 to 96 k $\Omega$  upon elevating the *L. monocytogenes* concentration from  $10^1$  to  $10^8$  CFU/mL. This situation has immediate consequences on the double layer capacitance  $C_{dl}$ . It can also be observed, in Figure 3a, that  $C_{dl}$  appears to decrease with an increase in bacterial concentration, which can be attributed to poor double layer charging at higher concentrations facilitated by reduced electron transfer (high  $R_{ct}$ ) at the electrode/electrolyte interface. The Randles circuit, shown in the inset in Figure 3a, was employed to obtain approximate estimates of the interfacial parameters involved in the *L. monocytogenes* sensing scenario by curve fitting of the Nyquist spectra of Figure 3a using Zview software. The latter is highlighted in Figure 3b, while the values of various interfacial parameters are listed in Table 1.

**Table 1.** A chart highlighting the approximate values of various interfacial parameters modeled by Randles circuit using Zview software.

SI No.	Listeria Concentration (CFU/mL)	$R_s$ ( $\Omega$ )	$R_{ct}$ ( $\Omega$ )	CPE (F)	$W_s$ ( $\Omega$ )
1	$10^1$	$5 \times 10^3$	$58 \times 10^3$	$2 \times 10^{-6}$	$1 \times 10^2$
2	$10^8$	$5 \times 10^3$	$96 \times 10^3$	$5 \times 10^{-9}$	$6 \times 10^2$

It can be observed from the above table that an increase in  $R_{ct}$  from 58 to 96 k $\Omega$  has a drastic impact on  $C_{dl}$ , as indicated in by the three-fold increase from 2  $\mu$ F to 5 nF, as the *L. monocytogenes* concentration is scaled up from  $10^1$  to  $10^8$  CFU/mL. As mentioned above, this is primarily due to poor double layer charging, since fewer electrons traverse the interface region due to the increased binding of the target and probe aptamer on the electrode surface. While the high-frequency bulk resistance remains constant at 5 k $\Omega$ , the diffusion impedance  $W_s$  increases from 0.1 to 0.6 k $\Omega$  due to steric hindrance between methylene blue and target aptamers at higher concentrations.

The calibration plot, obtained at a frequency of 120.45 kHz (Figure 3c) showed that  $R_{ct}$  increased linearly as the bacteria concentration was increased from  $10^1$  to  $10^8$  CFU/mL. These values also corresponded to the diameter of the semi-circle. The calibration plot (Figure 3b) verified the direct proportionality of  $R_{ct}$  and bacteria concentration, as it increased along with the concentration range from  $10^1$  to  $10^8$  CFU/mL. The limit of detection (LOD) and limit of quantification (LOQ) were graphically determined by the Meier and Zund method [22], i.e., 10.0 CFU/mL and 4.5 CFU/mL, respectively.

### 3.4. Selectivity of the Aptasensor

In order to validate the selectivity of the developed sensor, a sensing analysis was performed with various analytes. An interfering study with two different bacterial species, i.e., *E. coli* and *B. subtilis*, was conducted to validate the selectivity of the developed sensor. Figure 4 shows that each bacterium generates its own unique charge transfer response ( $R_{ct}$ ) with significant and specific deviations. Furthermore, a fixed concentration of *E. coli* and

*B. subtilis* ( $10^8$  CFU/mL) was individually mixed with *L. monocytogenes* ( $10^8$  CFU/mL) and the  $R_{ct}$  values of these mixtures were recorded at a calibration frequency of 120.45 kHz. As shown in Figure 4, the  $R_{ct}$  value for *L. monocytogenes* alone and the mixtures with *E. coli* and *B. subtilis* were  $\sim 95.1 \pm 3.8$ ,  $97.2 \pm 3.5$ , and  $93.8 \pm 3.9$  k $\Omega$ , respectively. These results indicate that irrespective of the presence of different bacteria in the sample, the developed sensor can accurately detect the presence of *L. monocytogenes*, which is attributed to its selective binding with the aptamer sequence. Therefore, from the result, it is concluded that the aptasensor responds selectively to *L. monocytogenes*.

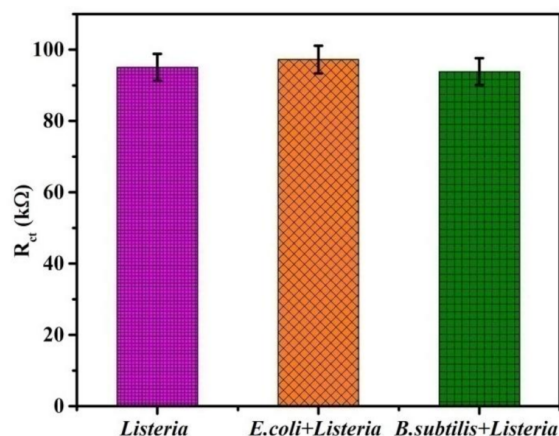


**Figure 4.** Impedance response of various bacteria indicating the selective nature of the developed sensor (L = *L. monocytogenes*, *E. coli* + *L. monocytogenes*, *B. subtilis* + *L. monocytogenes*), at 120.45 kHz.

### 3.5. Reproducibility and Storage Stability

Reproducibility of the ePAD was also studied and the coefficients of variation of four electrodes were tested and determined to be  $52.503 \text{ k}\Omega \pm 1.18\%$  (mean of  $R_{ct} \pm \text{COV}$ , within the batch) and  $58.365 \text{ k}\Omega \pm 5.54\%$  (mean of  $R_{ct} \pm \text{COV}$ , between the batch). The developed sensor was also tested for its stability and shelf-life. The impedance response of the sensor was recorded at a concentration of  $10^1$  CFU/mL for 20 days (Figure 5) at a regular interval of 5 days. The observed average value of impedance was found to be  $\sim 64.4 \pm 6.4$  k $\Omega$ ; and further, it indicated that the impedance changed insignificantly for 15 days, suggesting that the sensor gives stable impedance response over a period of 15 days.

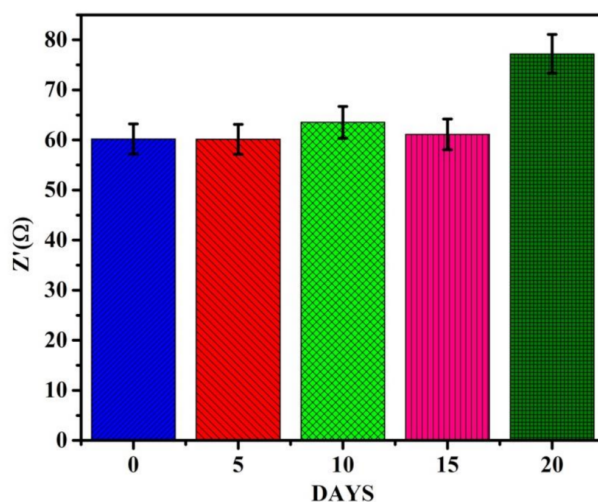


**Figure 5.** Stability and shelf-life study indicating a stable lifetime of 15 days.

### 3.6. Application of the Aptasensor in Real Sample Analysis

The validation of our aptasensor was analyzed by spiking milk and cheese with bacteria concentrations of  $10^1$ ,  $10^3$ , and  $10^5$  CFU/mL. The bar graph below (Figure 6) indicates that interfacial charge transfer resistance in spiked milk and cheese samples differs insignificantly as compared with that observed for the target. The minor increment in impedance observed for spiked cheese and milk for the target may be attributed to the former being insulating in nature, contrary to what is observed for the latter, which is suspended in a conducting electrolyte (MB/KCl). Furthermore, Table 2 shows the percentage recovery of bacteria in cheese and milk. Such high recovery proves the validation of the developed aptasensor.

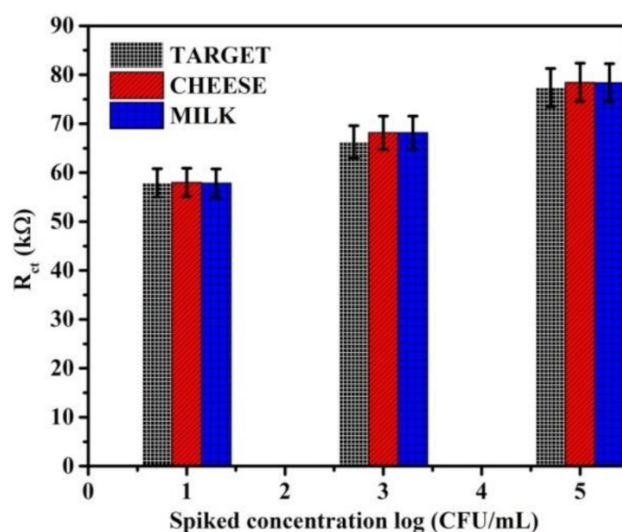


**Figure 6.** Charge transfer resistance observed for spiked cheese and milk. The response to bacteria is also shown for reference in 0.1 M KCl containing 0.1 mM methylene blue (frequency range of 100 Hz–10 MHz).

**Table 2.** Percentage recovery of bacteria concentrations in cheese and milk.

S. No.	Spiked Concentration (CFU/mL)	Cheese		Milk	
		Detected Concentration (CFU/mL)	% Recovery	Detected Concentration (CFU/mL)	% Recovery
1.	10	10.7	107	10.13	101.3
2.	1000	1023.1	102.3	1021.2	102.1
3.	100,000	104,712.8	104.7	100,461.5	100.4

## 4. Conclusions

In the present work, we demonstrated the feasibility of a paper-based platform utilizing  $WS_2$  for the detection of foodborne pathogens. An electrochemical sensor based on a  $WS_2$ /aptamer hybrid was successfully fabricated to detect *Listeria*. Impedance spectroscopy was performed using a two-electrode system. The use of the paper-based platform reduced the cost of the sensor fabrication and the volume of the analyte required. The linear range for the detection of *Listeria* was  $10^1$ – $10^8$  CFU/mL with a detection limit of 10.0 CFU/mL. The constructed aptasensor demonstrated high selectivity, reproducibility, and sensitivity toward *L. monocytogenes*. Due to the impressive detection limits and linear range, the developed sensor can be implemented in real-time field applications.

**Author Contributions:** Conceptualization, J.N. and S.J.; methodology, A.M. (Annu Mishra); software, A.M. (Ashish Mathur); validation, R.P. and J.N. and M.K.; formal analysis, S.R.; investigation, J.N.; resources, M.K.; data curation, A.M. (Annu Mishra); writing—A.M. (Annu Mishra); original draft Conceptualization, J.N. and S.J.; methodology, A.M. (Annu Mishra); software, A.M. (Ashish Mathur); validation, R.P. and J.N. and M.K.; formal analysis, S.R.; investigation, J.N.; resources, M.K.; data curation, A.M. (Annu Mishra); writing—A.M. (Annu Mishra); original draft preparation, A.M. (Annu Mishra) and S.R.; writing—review and editing, S.R. and A.M. (Annu Mishra); visualization, J.N.; supervision, R.P.; project administration, A.M. (Annu Mishra); funding acquisition, M.K. All authors have read and agreed to the published version of the manuscript.

**Funding:** This research received no external funding.

**Institutional Review Board Statement:** Not applicable.

**Informed Consent Statement:** Not applicable.

**Data Availability Statement:** We have not reported any data where supporting reported results can be found.

**Acknowledgments:** The present work received support to M.K. from the Science and Engineering Research Board (SERB) No. ECR/2017/001222 and the University Grant Commission (UGC) No.F.4-5(201 FRP)/2015(BSR).

**Conflicts of Interest:** The authors declare no conflict of interest.

## References

1. World Health Organization, Food Safety. 2019. Available online: <https://www.who.int/news-room/fact-sheets/detail/food-safety> (accessed on 4 June 2019).
2. Chiu, C.H.; Wu, T.L.; Su, L.H.; Chu, C.; Chia, J.H.; Kuo, A.J.; Chien, M.S.; Lin, T.Y. The emergence in Taiwan of fluoroquinolone resistance in *Salmonella enterica* Serotype Choleraesuis. *N. Engl. J. Med.* **2002**, *346*, 413–419. [[CrossRef](#)] [[PubMed](#)]
3. Centers for Disease Control and Prevention. Available online: <https://www.cdc.gov/listeria/faq.html> (accessed on 12 December 2016).
4. Bagheryan, Z.; Raoof, J.B.; Golabi, M.; Turner, A.P.F.; Beni, V. Diazonium-based impedimetric aptasensor for the rapid label-free detection of *Salmonella typhimurium* in food sample. *Biosens. Bioelectron.* **2016**, *80*, 566–573. [[CrossRef](#)] [[PubMed](#)]
5. Heredia, N.; Garcia, S. Animals as sources of food-borne pathogens: A review. *Anim. Nutr.* **2018**, *4*, 250–255. [[CrossRef](#)] [[PubMed](#)]
6. Law, J.W.-F.; Ab Mutalib, N.S.; Chan, K.G.; Lee, L.H. Rapid methods for the detection of foodborne bacterial pathogens: Principles, applications, advantages and limitations. *Front. Microbiol.* **2014**, *5*, 770. [[CrossRef](#)] [[PubMed](#)]
7. Cho, I.H.; Ku, S. Current technical approaches for the early detection of foodborne pathogens: Challenges and opportunities. *Int. J. Mol. Sci.* **2017**, *18*, 2078. [[CrossRef](#)] [[PubMed](#)]
8. Grieshaber, D.; MacKenzie, R.; Vörös, J.; Reimhult, E. Electrochemical biosensors—Sensor principles and architectures. *Sensors* **2008**, *8*, 1400–1458. [[CrossRef](#)] [[PubMed](#)]
9. Singh, K.; Chauhan, R.; Solanki, P.R.; Basu, T. Development of impedimetric biosensor for total cholesterol estimation based on polypyrrole and platinum nanoparticle multi layer nanocomposite. *Int. J. Org. Chem.* **2013**, *3*, 262–274. [[CrossRef](#)]
10. Mathur, A.; Gupta, R.; Kondal, S.; Wadhwa, S.; Pudake, R.N.; Shivani Kansal, R.; Pundir, C.S.; Narang, J. A new tactics for the detection of *S. aureus* via paper based geno-interface incorporated with graphene nano dots and zeolites. *Int. J. Biol. Macromol.* **2018**, *112*, 364–370. [[CrossRef](#)] [[PubMed](#)]
11. Sidhu, R.J.; Claussen, J.; Rong, Y.; Mclamore, E. Smart Biomedical and Physiological Sensor Technology XII. In Proceedings of the SPIE Sensing Technology + Applications, Baltimore, MD, USA, 20–24 April 2015.
12. Singhal, C.; Dubey, A.; Mathur, A.; Pundir, C.S.; Narang, J. Paper based DNA biosensor for detection of chikungunya virus using gold shells coated magnetic nanocubes. *Process Biochem.* **2018**, *74*, 35–42. [[CrossRef](#)]
13. Ashraf, W.; Fatima, T.; Srivastava, K.; Khanuja, M. Superior photocatalytic activity of tungsten disulfide nanostructures: Role of morphology and defects. *Appl. Nanosci.* **2019**, *9*, 1–15. [[CrossRef](#)]
14. Narang, J.; Singhal, C.; Khanuja, M.; Mathur, A.; Jain, A.; Pundir, C.S. Hydrothermally synthesized zinc oxide nanorods incorporated on lab-on-paper device for electrochemical detection of recreational drug. *Artif. Cells Nanomed. Biotechnol.* **2018**, *46*, 1586–1593. [[CrossRef](#)] [[PubMed](#)]
15. Cao, S.; Liu, T.; Hussain, S.; Zeng, W.; Peng, X.; Pan, F. Synthesis and characterization of novel chrysanthemum-like tungsten disulfide (WS<sub>2</sub>) nanostructure: Structure, growth and optical absorption property. *Mater. Lett.* **2014**, *129*, 205–208. [[CrossRef](#)]
16. Ghorai, A.; Bayan, S.; Gogurla, N.; Midya, A.; Ray, S.K. Highly luminescent WS<sub>2</sub> quantum Dots/ZnO heterojunctions for light emitting devices. *ACS Appl. Mater. Interfaces* **2016**, *9*, 558–565. [[CrossRef](#)] [[PubMed](#)]
17. Lvovich, V.F. Fundamentals of electrochemical impedance spectroscopy. In *Impedance Spectroscopy*; Wiley: New York, NY, USA, 2012; pp. 1–21.

18. Mathur, A.; Nayak, H.C.; Rajput, S.; Roy, S.; Nagabooshanam, S.; Wadhwa, S.; Kumar, R. An enzymatic multiplexed impedimetric sensor based on  $\alpha$ -MnO<sub>2</sub>/GQD nano-composite for the detection of diabetes and diabetic foot ulcer using micro-fluidic platform. *Chemosensors* **2021**, *9*, 339. [[CrossRef](#)]
19. Khanna, M.; Roy, S.; Kumar, R.; Wadhwa, S.; Mathur, A.; Dubey, A.K. MnO<sub>2</sub> based bisphenol—A electrochemical sensor using micro-fluidic platform. *IEEE Sens. J.* **2018**, *18*, 2206–2209. [[CrossRef](#)]
20. Roy, S.; John, A.; Nagabooshanam, S.; Mishra, A.; Wadhwa, S.; Mathur, A.; Narang, J.; Singh, J.; Dilawar, N.; Davis, J. Self-aligned TiO<sub>2</sub>—Photo reduced graphene oxide hybrid surface for smart bandage application. *Appl. Surf. Sci.* **2019**, *488*, 261–268. [[CrossRef](#)]
21. Ma, X.; Jiang, Y.; Jia, F.; Yu, Y.; Chen, J.; Wang, Z.J. An aptamer-based electrochemical biosensor for the detection of Salmonella. *Microbiol. Methods* **2014**, *98*, 94–98. [[CrossRef](#)] [[PubMed](#)]
22. Meier, P.C.; Zünd, R.E. *SMAC-Statistical Methods in Analytical Chemistry*; Wiley Analytical Science, Wiley: New York, NY, USA, 2000; p. 153. ISBN 978-0-471-72611-1.